Check for updates

RESEARCH ARTICLE

NANO · MICRO small
www.small-journal.com

# 3D-Continuous Nanoporous Covalent Framework Membrane Nanoreactors with Quantitatively Loaded Ultrafine Pd Nanocatalysts

*Dawoon Jeong, Wangsuk Oh, and Ji-Woong Park**

**The confinement effect of catalytic nanoreactors containing metal catalysts within nanometer-sized volumes has attracted significant attention for their potential to enhance reaction rate and selectivity. Nevertheless, unregulated catalyst loading, aggregation, leaching, and limited reusability remain obstacles to achieving an efficient nanoreactor. A robust and durable catalytic membrane nanoreactor prepared by incorporating palladium nanocatalysts within a 3D-continuous nanoporous covalent framework membrane is presented. The reduction of palladium precursor occurs on the pore surface within 3D nanochannels, producing ultrafine palladium nanoparticles (Pd NPs) with their number density adjustable by varying metal precursor concentrations. The precise catalyst loading enables controlling the catalytic activity of the reactor while preventing excess metal usage. The facile preparation of Pd NP-loaded free-standing membrane materials allows hydrodechlorination in both batch and continuous flow modes. In batch mode, the catalytic activity is proportional to the loaded Pd amount and membrane area, while the membrane retains its activity upon repeated use. In continuous mode, the conversion remains above 95% for over 100 h, with the reactant solution passing through a single 50 µm-thick Pd-loaded membrane. The efficient nanoporous film-type catalytic nanoreactor may find applications in catalytic reactions for small chemical devices as well as in conventional chemistry and processes.**

## 1. Introduction

Performing a chemical reaction within a confined space on a nanoscale (called a nanoreactor) can improve reaction efficiency and selectivity.[1,2] This is achieved by limiting the diffusion of molecules beyond the small space of the nanoreactor, which differs from bulk solutions.[3–9] Nanocatalysts are typically housed within the nanoreactor voids, and the process of creating catalytic metal nanoreactors involves filling the voids with precursor material and subsequent reduction.

Nanoreactors employing hollow particles,[10,11] micelles,[12,13] or dendrimers[14,15] can be mixed homogeneously with reactants in their colloidal dispersions. These nanoparticles possess small compartments for guest encapsulation and catalysis. Nevertheless, the retrieval and reuse of these nanoreactors present significant challenges, and the stabilizing agents employed may potentially diminish catalytic activity.[16] Alternatively, anchoring nanocatalysts onto solid nanoporous substrates can yield reusable heterogeneous catalytic nanoreactors. In such instances, creating a uniform nanopore structure over a substantial surface area is crucial. It is imperative to prevent particle aggregation or pore-clogging during the loading of nanocatalysts. Furthermore, these substrates must maintain their structure while undergoing catalyst loading or chemical reactions involving organic solvents and reagents.

The process for creating metal nanoparticles (MNPs)-loaded nanoreactors typically involves the chemical or thermal reduction of metal precursors contained within the pores of hosts or substrates.[17] However, conventional methods often result in excessive metal consumption during precursor loading, leading to uncontrolled sizes of metal particles either inside or outside the nanopores. Achieving precise control over the quantity of metal loaded into the pores while ensuring uniform distribution of nanoparticles throughout the entire structure has been challenging. Hence, the development of a novel nanoreactor that utilizes only the necessary amount of metal precursor and enables precise control of nanocatalyst size and quantity is highly desirable.

Free-standing membranes with interconnected nanopores in 3D configurations offer an alternative nanoreactor format.[18] The continuous nanochannels within the membrane allow the precursor solution to come into contact with the pore surface at

D. Jeong, W. Oh, J.-W. Park
School of Materials Science and Engineering
Gwangju Institute of Science and Technology
123 Cheomdan-gwagiro, Bukgu, Gwangju 61005, South Korea
E-mail: jiwoong@gist.ac.kr

The ORCID identification number(s) for the author(s) of this article can be found under https://doi.org/10.1002/smll.202309490

© 2024 The Authors. Small published by Wiley-VCH GmbH. This is an open access article under the terms of the Creative Commons Attribution-NonCommercial-NoDerivs License, which permits use and distribution in any medium, provided the original work is properly cited, the use is non-commercial and no modifications or adaptations are made.

**DOI: 10.1002/smll.202309490**

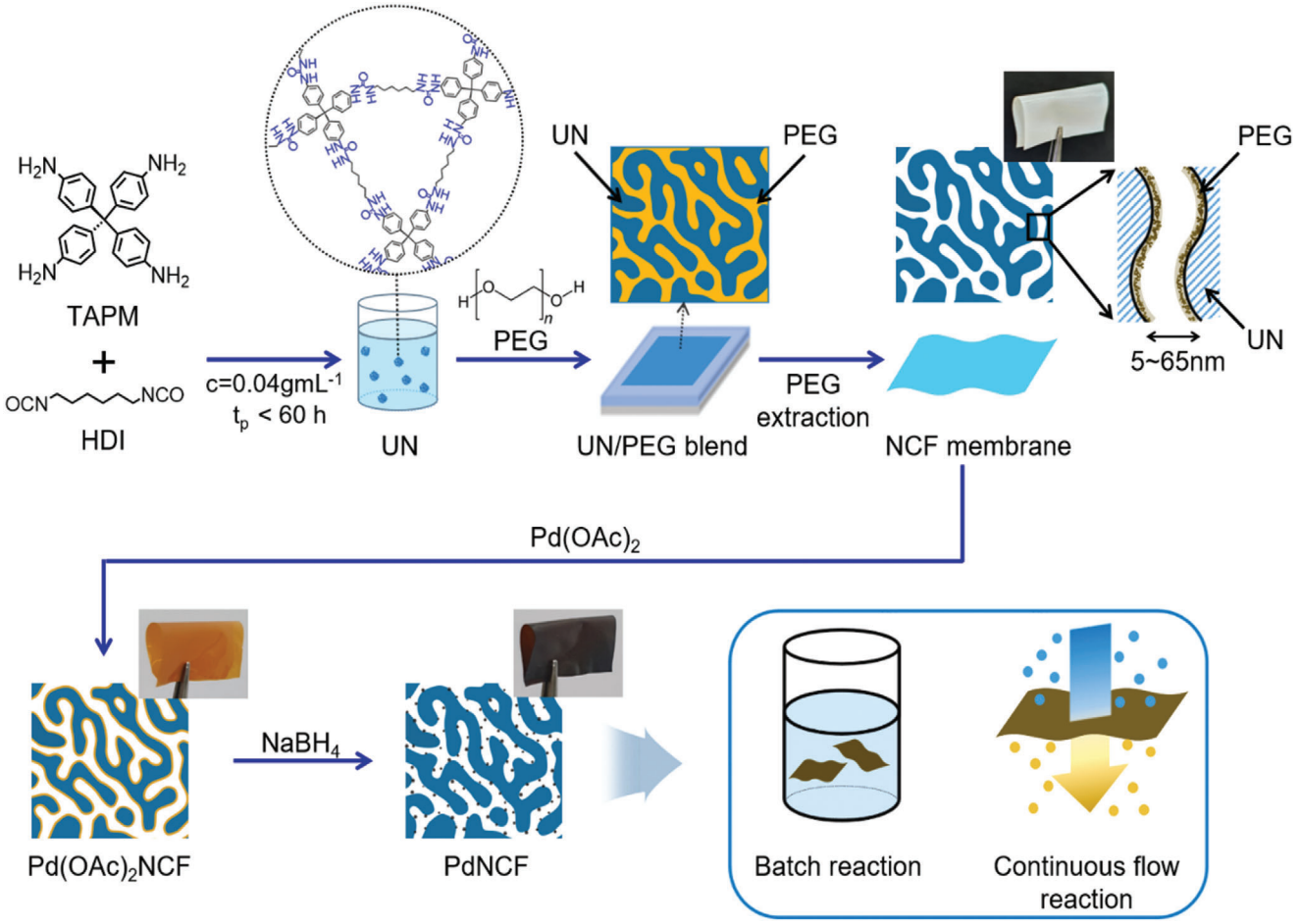


**Figure 1.** Schematic representation of the synthetic procedures for 3D-continuous NCF membranes with encapsulated Pd NPs within the nanopores. The photographs depict an as-prepared NCF, $Pd(OAc)_2$NCF, and PdNCF membrane sheets with a size of 1.5 × 1.5 $cm^2$ and a thickness of 45 ± 5 µm.

a uniform concentration, enabling the formation of nanocatalysts uniformly distributed across the membrane pore. The 3D nanopores facilitate efficient mass transfer between themselves and the surrounding solution, ensuring optimal reaction kinetics.[19–21]

However, conventional nanoporous polymer membranes, typically prepared by nonsolvent-induced phase separation (NIPS) or block copolymer microphase separation, come with significant limitations when applied to nanoreactor applications. The synthesis of large-area polymer membranes with 3D continuous nanopores of narrow and well-controlled size distribution is highly challenging. Additionally, these membranes lack sufficient resistance to organic chemicals, and their pore structures are susceptible to deformation when exposed to such substances, particularly over extended periods.[22–24]

The development of 3D-continuous nanoporous covalent frameworks (NCFs) has introduced an optimal platform for membrane-based catalytic nanoreactors.[25,26] By capturing bicontinuous spinodal microphase via sol-gel crosslinking polymerization and subsequently removing the soluble phase, these frameworks can form a 3D-continuous nanoporous structure with relatively uniform pore sizes in the tens-of-nanometer range. The molecular-level covalent network skeleton of the NCFs provides high dimensional stability, making them resistant to organic solvents and varying temperatures. NCF membranes are flexible, scalable, and suitable for various applications.

NCF membranes have demonstrated potential for biocatalysis by incorporating enzymes into the nanopores,[27,28] which has prompted interest in utilizing them for nanocatalyst-loaded nanoreactors. However, loading metal nanoparticles into the nanopores using the pressured flow method for loading enzymes faces limitations due to the absence of suitable techniques for dispersing nanoparticles without capping agents. Therefore, further research is necessary to develop effective strategies for preparing metal nanocatalyst-loaded NCFs while ensuring proper dispersion and stability of the nanoparticles within the nanopores.

In this study, a novel catalytic membrane nanoreactor is presented, incorporating Pd nanoparticles (NPs) encapsulated within the 3D-continuous nanopores of the NCF. The catalytic performance is demonstrated in a hydrodechlorination reaction as a model system. The concentration-dependent adsorption behaviors of the palladium precursor onto the continuous pore of the NCFs enable the number density of palladium nanoparticles to be adjusted by varying the concentration. The flexibility in regulating metal loadings and sheet sizes enhances


© 2024 The Authors. Small published by Wiley-VCH GmbH

16136829, 2024, 29, Downloaded from https://onlinelibrary.wiley.com/doi/10.1002/smll.202309490 by Gwangju Institute Of Science, Wiley Online Library on [01/04/2026]. See the Terms and Conditions (https://onlinelibrary.wiley.com/terms-and-conditions) on Wiley Online Library for rules of use; OA articles are governed by the applicable Creative Commons License

the scalability of catalyst quantity, making the membranes suitable for both batch and flow reactions. The catalytic membrane nanoreactors exhibit exceptional stability over multiple long-term reuses. These results showcase the effectiveness of 3D-continuous NCF membranes as platforms for catalytic nanoreactors. They enable the realization of efficient, stable, and reusable catalysts with precisely controlled activity for various catalytic processes.

## 2. Results and Discussion

### 2.1. Preparation of Pd NP-Loaded NCF Membranes

The synthetic procedures for preparing NCF membranes and incorporating Pd NPs onto the membrane are presented in **Figure 1** (for further details, refer to the Experimental Section). The NCF membranes were synthesized following the reported method.[25,27,28] In summary, a solution containing tetrakis(4-aminophenyl)methane (TAPM) and hexamethylene diisocyanate (HDI) in N, N-dimethylformamide (DMF) at a concentration of 0.04 g $mL^{-1}$ was polymerized. The resulting polyurea network (UN) sol was then mixed with polyethylene glycol (PEG), cast into films, and subsequently subjected to water extraction to remove PEG. This process yielded 3D-continuous NCF membranes with an average pore size of 38 nm, ranging from 5 to 65 nm. As reported previously, the pore surface of the NCF is coated with PEG brushes bounded to the framework of the urea network through urethane bonds.[27,28] We expected the PEG brushes to facilitate the adsorption of Pd compounds or nanoparticles within the nanopores like free or particle-bound PEGs do,[29–31] yielding Pd/PEG catalytic layer coated onto the 3D continuous nanochannels.

The catalyst was loaded onto the NCF membrane by immersing it in the $Pd(OAc)_2$ solution in acetone. The resulting membrane, $Pd(OAc)_2$NCF, has $Pd(OAc)_2$ adsorbed onto the 3D-continuous nanoporous channels. Subsequently, the reduction of $Pd(OAc)_2$ was carried out by immersing the $Pd(OAc)_2$NCF membrane in an aqueous $NaBH_4$ solution, leading to the formation of a PdNCF through the generation of Pd NPs within the nanopores.

The ability to precisely adjust the Pd loadings in the membrane is crucial for fine control of the catalytic activity of the PdNCF membrane. We found that $Pd(OAc)_2$ adsorption onto the NCF reached the saturation limit in 2 h, which varied with the $Pd(OAc)_2$ concentration in the adsorption solution.[32] The adsorption dependence on the solution concentrations followed the Langmuir adsorption isotherm (**Figure 2**; Figures S1 and S2, Supporting Information). The adsorption capacity of $Pd(OAc)_2$ at equilibrium ($q_e$, mmol $g^{-1}$) was estimated by analyzing the change in UV–vis absorbance (See Experimental Section and Figure S1, Supporting Information). The Pd content in the PdNCF could also be measured by the inductively coupled plasma optical emission spectrometer (ICP-OES), which agreed well with the UV–vis-based estimation (Figure 2).

The Langmuir adsorption behavior indicates that the NCF nanochannel provided homogeneous adsorption sites.[33,34] This standard adsorption behavior onto the NCF ensures the loading of metal in a precise quantity by varying the concentration of the precursor adsorbates. Moreover, the residual precursor

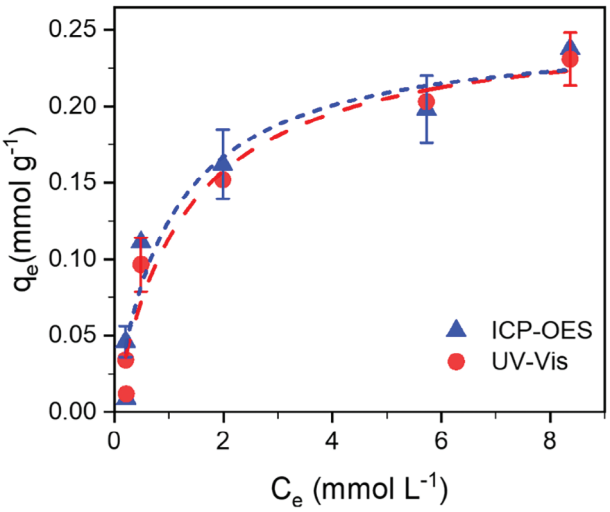


**Figure 2.** Adsorption isotherms of $Pd(OAc)_2$ onto the NCF membranes at different concentrations at equilibrium ($C_e$, mmol $L^{-1}$). Points are estimated by ICP-OES (blue) and UV–vis (red). Dashed lines show Langmuir adsorption isotherms.

molecules in the solution after adsorption onto one membrane remain intact and thus can be reused for adsorption onto new membranes, effectively preventing excessive metal usage.

All characterization data consistently indicate that the Pd NPs were quantitatively and uniformly incorporated into the 3D nanochannels of the NCF. The porous structure of the initial NCF membrane remains unchanged throughout the precursor loading, rinsing, and reduction process involving organic solvents. The scanning electron microscopy (SEM, **Figure 3b**) and transmission electron microscopy (TEM, Figure 3d) of the membrane cross-sections of the PdNCF revealed that they possessed the continuous nanoporous structure inherent to the bare NCF membrane (Figure 3a,c) without clogging or deformation. In particular, the TEM images of the PdNCF (Figure 3d) clearly displayed interconnected nanopores adorned with well-dispersed, fine Pd NPs, which had a size in the range of 1.0–2.0 nm. Furthermore, scanning electron microscopy with energy dispersive X-ray spectroscopy (SEM-EDX) spectrum and mapping analysis of the PdNCF membrane (Figure S3, Supporting Information) exhibited the uniform distribution of Pd NPs throughout the membrane's thickness.

The formation of Pd NPs is further confirmed through X-Ray Diffraction (XRD) analysis (Figure S4, Supporting Information). In the PdNCF-1.0 membrane (PdNCF with 1.0 wt% of Pd), no distinctive peaks are observed due to the low content of ultra-small Pd NPs. However, the PdNCF-5.3 membrane exhibits weak Pd (111) and (200) peaks at $2\theta$ = 39.2° and 45.6°, respectively.[35]

The Barrett–Joyner–Halenda (BJH)-based pore size distribution analysis of the NCF and PdNCF membranes with varying amounts of Pd contents (Figure 3e) indicates that the distribution curves shifted toward smaller pore sizes as the Pd contents increased. In the X-ray photoelectron spectroscopy (XPS) spectra of the PdNCF membrane (Figure 3f), the relative peak area ratio of $Pd^0$ $3d_{5/2}$ (335.9 eV) to $Pd^{2+}$ $3d_{5/2}$ (337.8 eV) was 3.14, confirming the formation of Pd NPs by simply dipping the


© 2024 The Authors. Small published by Wiley-VCH GmbH

16136829, 2024, 29, Downloaded from https://onlinelibrary.wiley.com/doi/10.1002/smll.202309490 by Gwangju Institute Of Science, Wiley Online Library on [01/04/2026]. See the Terms and Conditions (https://onlinelibrary.wiley.com/terms-and-conditions) on Wiley Online Library for rules of use; OA articles are governed by the applicable Creative Commons License

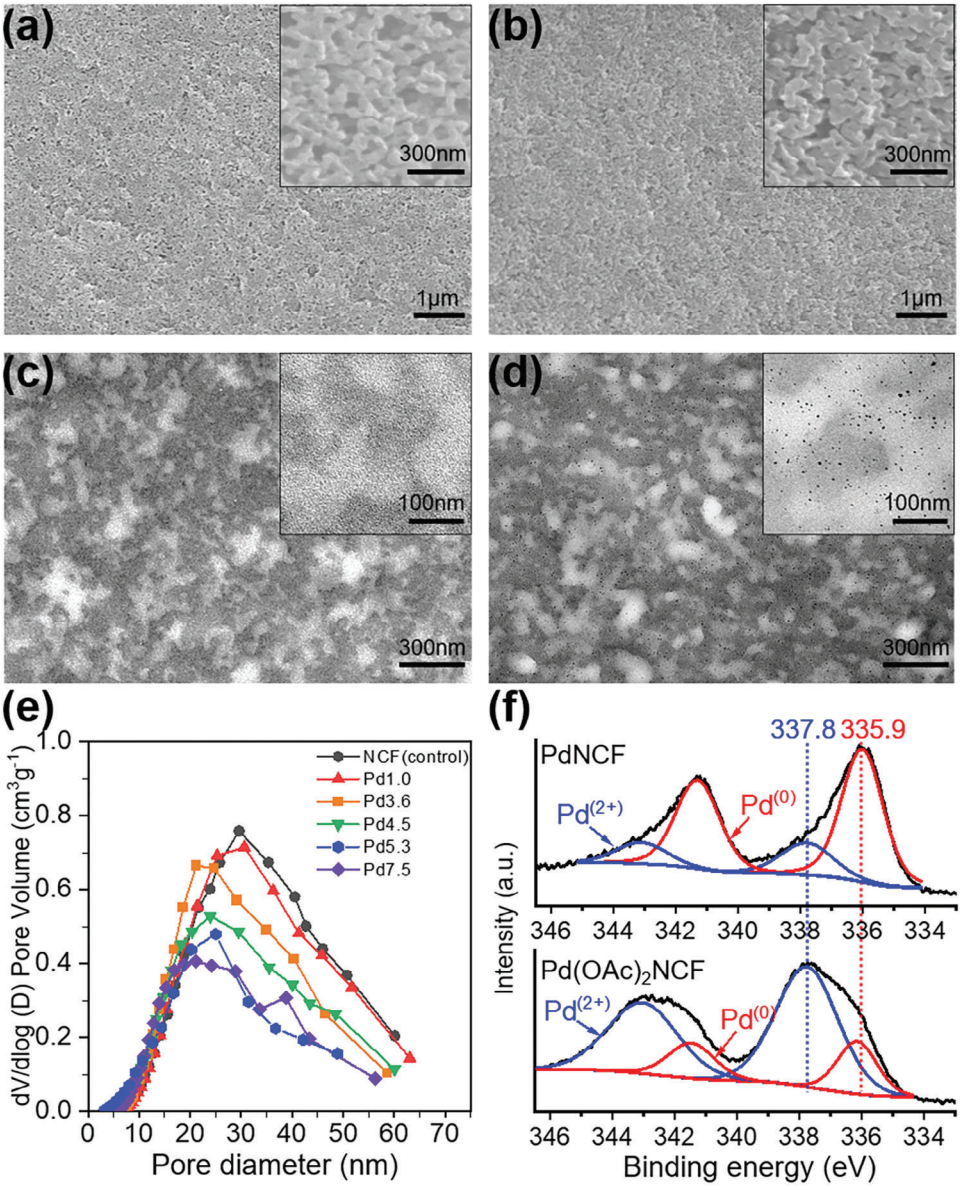


**Figure 3.** Cross-sectional a,b) SEM and c,d) FE-TEM images of an a,c) NCF and b,d) PdNCF membrane (For TEM measurements, the membrane was microtomed into 80–100 nm-thick sections and images were obtained without staining). e) BJH pore size distribution of NCF(control) and PdNCF membranes with varying Pd contents (wt%). NCF(control) was prepared by immersion of the NCF (as-prepared) in acetone for 6 h, followed by drying. f) Pd 3d XPS spectra for $Pd(OAc)_2$NCF and PdNCF. The PdNCF for (b,d, and f) contained Pd of 5.3 wt%. The NCF membrane was immersed in a 20 mM $Pd(OAc)_2$ solution, dried, and then immersed in a 20 mM $NaBH_4$ solution (See Experimental Section for details).

$Pd(OAc)_2$NCF membrane into the $NaBH_4$ solution. The residual $Pd^{2+}$ peak in the PdNCF may be attributed to the partial formation of PdO.[36,37]

The PdNCF membrane sheets obtained from different $Pd(OAc)_2$ concentrations exhibited different colors, indicating their difference in Pd loadings (Figure S5, Supporting Information). **Table 1** shows that the Pd loading, Brunauer–Emmett–Teller (BET) specific surface area, pore volume, average pore diameter, and the average Pd NP size in the PdNCF-X, where X represents the weight percent of Pd. The ICP-OES-measured Pd loadings of the PdNCF-X membranes were estimated to be 1.0 to 7.5 wt%, as the $Pd(OAc)_2$ concentrations varied from 0.1 to 30 mM. The specific surface area and pore diameter of the PdNCF decreased with the increase in the amount of Pd NPs within the nanopores.

In the PdNCF-7.5, obtained from the adsorption concentration near the saturation limit in the adsorption isotherm, the ratio of the $C_2H_4O$ unit of PEG to the Pd atom was estimated to be ≈5. The ratio increased to much greater than 5 as the concentration of the adsorption solution was lowered below the saturation limit, indicating that a sufficient number of PEG binding sites were available for the adsorption of the Pd precursor throughout the concentration range used in the current study.


© 2024 The Authors. Small published by Wiley-VCH GmbH

16136829, 2024, 29, Downloaded from https://onlinelibrary.wiley.com/doi/10.1002/smll.202309490 by Gwangju Institute Of Science, Wiley Online Library on [01/04/2026]. See the Terms and Conditions (https://onlinelibrary.wiley.com/terms-and-conditions) on Wiley Online Library for rules of use; OA articles are governed by the applicable Creative Commons License

**Table 1.** Characteristics of the NCF and PdNCF pore structures.

| Sample[a] | Pd [wt%][b] | Concentration of $Pd(OAc)_2$ [mM][c] | BET surface area [$m^2\ g^{-1}$] | Pore volume [$cm^3\ g^{-1}$][d] | Pore diameter [nm][d] | Particle size [nm][e] |
|---|---|---|---|---|---|---|
| NCF (as-prepared) | 0 | – | 42.4 | 0.43 | 34.0 | – |
| NCF (control)[f] | 0 | 0 | 43.5 | 0.37 | 33.8 | – |
| PdNCF-1.0 | 1.0 ± 0.1 | 1.0 | 36.7 | 0.34 | 33.0 | 1.2 ± 0.8 |
| PdNCF-3.6 | 3.6 ± 0.4 | 5.0 | 35.1 | 0.32 | 28.6 | 1.4 ± 0.6 |
| PdNCF-4.5 | 4.5 ± 0.3 | 10.0 | 31.5 | 0.28 | 29.0 | 1.6 ± 1.3 |
| PdNCF-5.3 | 5.3 ± 0.1 | 20.0 | 27.7 | 0.27 | 25.6 | 1.5 ± 1.2 |
| PdNCF-7.5 | 7.5 ± 0.1 | 30.0 | 27.0 | 0.23 | 26.9 | 1.8 ± 1.1 |

[a] X is Pd loading in wt% in each PdNCF-X membrane; [b] Pd loading X (wt%) of each PdNCF was measured by ICP-OES; [c] $Pd(OAc)_2$ concentration in the adsorption solution; [d] Pore volume and average pore diameter were analyzed by the BJH method from the desorption branch of the $N_2$ sorption isotherm; [e] Average particle size was estimated using ImageJ for more than 1000 palladium nanoparticles; [f] The NCF (control) was prepared by immersion of the as-prepared NCF in pure acetone for the duration (6 h) used for Pd adsorption, followed by drying for porosity measurement.

The analysis of TEM images (**Figure 4**; Figure S6, Supporting Information) of PdNCF-X indicates that the average Pd NP size was changed only slightly by different Pd loadings. High-resolution TEM images revealed that the dimensions of Pd nanoparticles were within the 1–2 nm range (Figure 4e,f, Table 1). The TEM images also show that, instead of the size, the number density of Pd NPs increased with Pd loadings. This observation suggests that the higher number of $Pd(OAc)_2$ adsorbed onto the pore surface leads to a greater density of nucleation events. The relatively uniform particle size indicates that the growth of nuclei into NPs was limited by the slow diffusion of metal atoms on the pore surface, which the strong interaction between Pd and the PEG chains may cause. The growth of NPs follows a different trend in a solution, where higher metal ion concentrations would result in a faster growth rate and the formation of larger nanoparticles.[38] The homogeneous distribution of fine Pd NPs within the nanopore structure was maintained across a wide range of reducing agent ($NaBH_4$) concentrations. Nevertheless, when the reduction is carried out at excessively high $NaBH_4$ concentrations, agglomerates of small Pd NPs are formed (Figure S7, Supporting Information).

## 2.2. Hydrodechlorination Catalyzed with PdNCF Nanoreactor

### *2.2.1. Batch Catalytic Reaction with PdNCF*

Chlorine-containing aromatic compounds have become a significant environmental concern in recent times.[39–41] Hydrodechlorination (HDC) has proven to be a convenient method for the

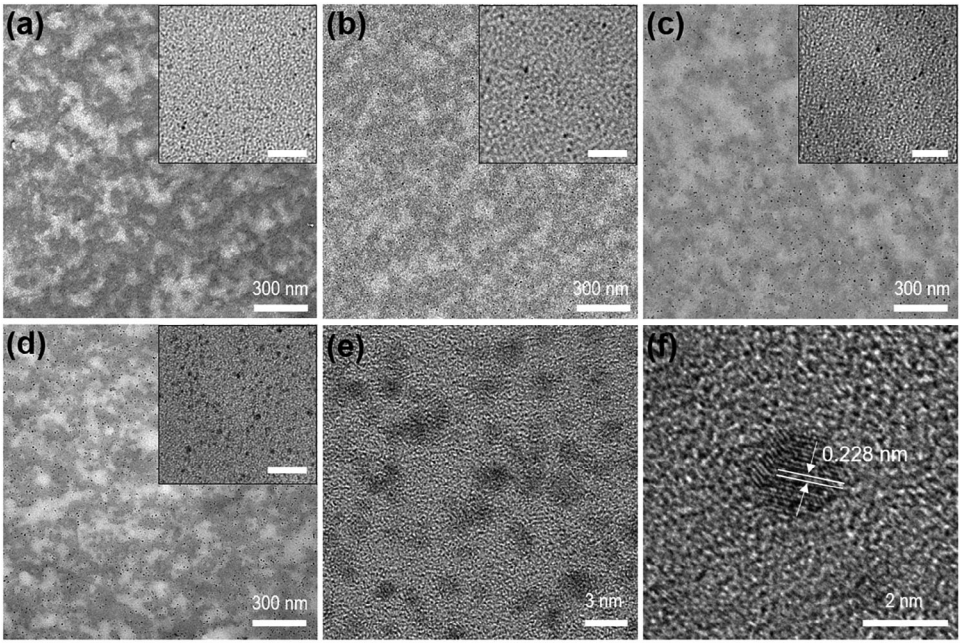


**Figure 4.** Cross-sectional TEM images of PdNCF-X membranes with different Pd loadings. a–d) PdNCF-0.14, 1.0, 4.5, and 5.3, were obtained from $Pd(OAc)_2$ concentrations of 0.1, 1.0, 10, and 20 mM, respectively. The scale bar in the insets is 20 nm. e,f) High-resolution TEM images of (d). The images were obtained for ultrathin sections of the PdNCF membrane with a thickness of 80–100 nm.


© 2024 The Authors. Small published by Wiley-VCH GmbH

16136829, 2024, 29, Downloaded from https://onlinelibrary.wiley.com/doi/10.1002/smll.202309490 by Gwangju Institute Of Science, Wiley Online Library on [01/04/2026]. See the Terms and Conditions (https://onlinelibrary.wiley.com/terms-and-conditions) on Wiley Online Library for rules of use; OA articles are governed by the applicable Creative Commons License

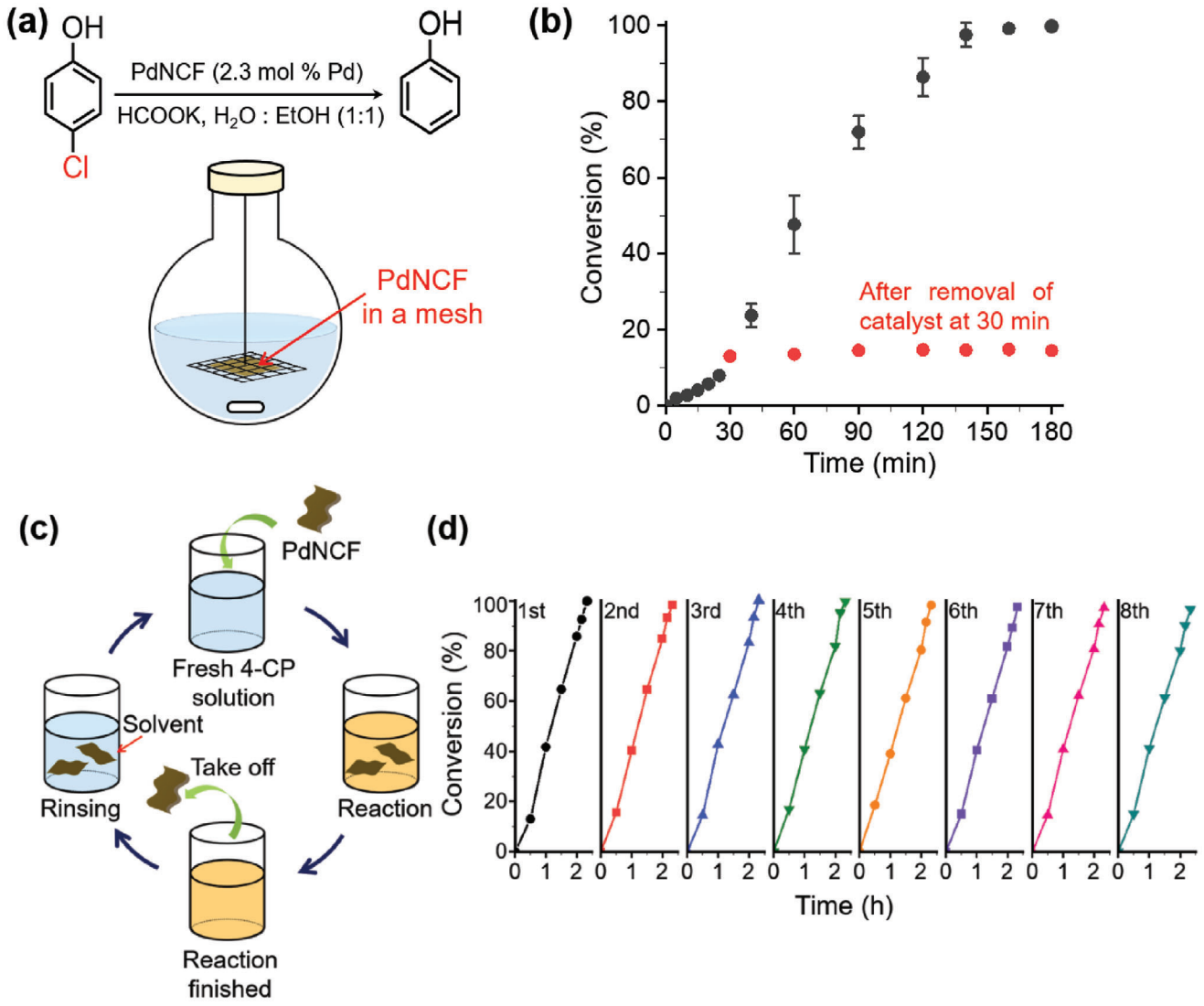


**Figure 5.** Batch mode catalytic reaction with PdNCF nanoreactor. a) A hydrodechlorination (HDC) of 4-CP in a laboratory flask with PdNCF enclosed in a stainless steel mesh. b) The conversion versus time plots in the presence of the PdNCF catalyst and after its removal at 30 min. c) Recycling of PdNCF membrane for multiple batches. d) Conversion versus time plots for eight sequential HDC batches with a PdNCF-5.3 membrane section. The amount of Pd was set to be 2.3 mol% compared to 4-CP. The reaction was conducted at 40 °C in the solutions with 4-chlorophenol (0.4 mmol), HCOOK (6 mmol), $Et_3N$ (0.8 mmol), and EtOH: $H_2O$ (1:1, 20 mL).

dehalogenation of aryl halides due to its experimental simplicity and good yields. We employed a PdNCF membrane nanoreactor to convert 4-chlorophenol (4-CP) into phenol using potassium formate as a hydrogen donor dissolved in aqueous ethanol.[42,43] The formate ion is adsorbed on the Pd surface and then transformed into a hydride ion and carbon dioxide. The hydride ion attacks the C—Cl bond as adsorbed on the catalyst surface (Figure S8, Supporting Information).[43] Utilizing organic hydrogen donors for HDC eliminates the need for high-pressure hydrogen gas, allowing us to fine-tune the reaction conditions suitable for testing the PdNCF membrane nanoreactors.[44–46]

In batch reactions, a section of the PdNCF membrane held in a stainless steel mesh was immersed in a stirred mixture of reactants, as depicted in **Figure** 5a. Within 2.5 h, the conversion of 4-CP to phenol reached nearly 100%, which was validated through gas chromatography-mass spectrometry (GC-MS) analysis (Figure S9, Supporting Information). Notably, no further reaction occurred after removing the PdNCF sheets from the reaction solution, indicating the absence of catalyst leaching (Figure 5b). A brief induction period was observed initially, attributed to the time required for the solution to be adsorbed into the nanopore structure. The stability of PdNCF's activity against leaching enabled the catalyst to be reused multiple times. After completing one reaction batch, the PdNCF sheet was removed from the solution, rinsed with water and EtOH, and then immersed in a fresh reactant solution (Figure 5c). As demonstrated in Figure 5d, the PdNCF membrane catalyst exhibited consistent activity over eight catalytic cycles.

The 3D-continuous nanopore structure of the recovered PdNCF membrane nanoreactor remains unchanged compared


© 2024 The Authors. Small published by Wiley-VCH GmbH

16136829, 2024, 29, Downloaded from https://onlinelibrary.wiley.com/doi/10.1002/smll.202309490 by Gwangju Institute Of Science, Wiley Online Library on [01/04/2026]. See the Terms and Conditions (https://onlinelibrary.wiley.com/terms-and-conditions) on Wiley Online Library for rules of use; OA articles are governed by the applicable Creative Commons License

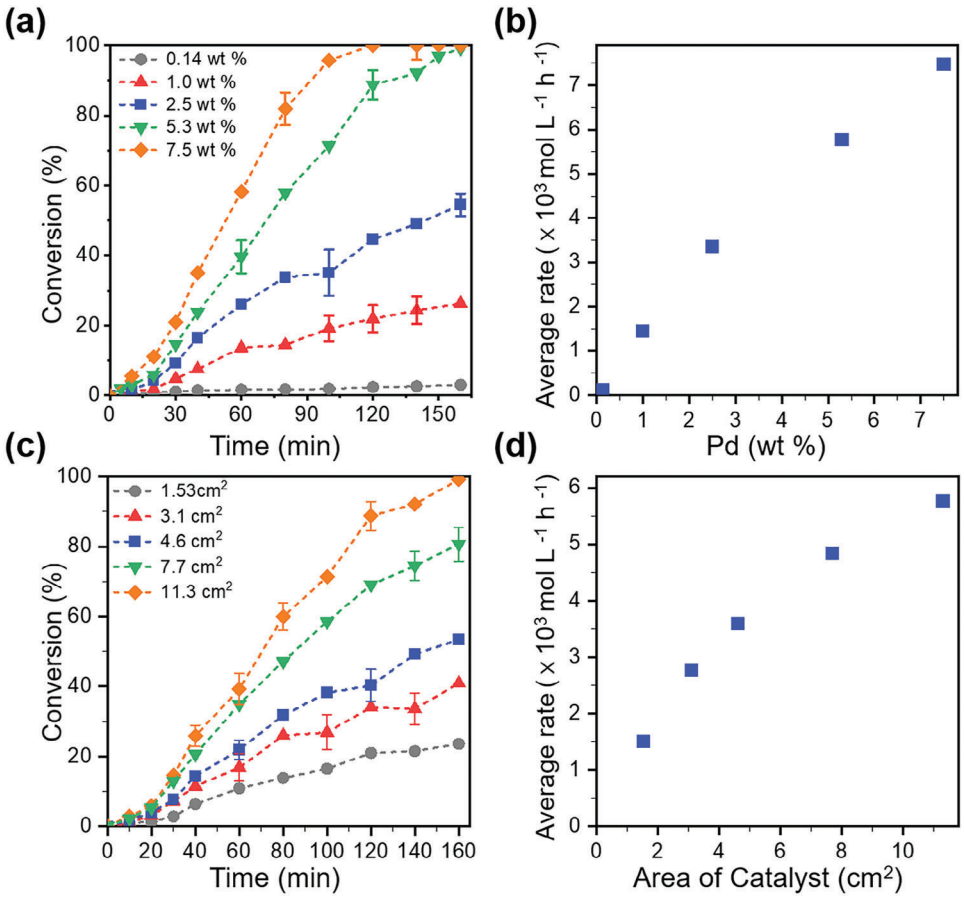


**Figure 6.** The rate of HDC reaction is adjustable with Pd loading and the area of PdNCF. a) The conversion versus time plot with different Pd loadings (wt%) in PdNCF with an area of 11.3 $cm^2$. b) The average reaction rate versus Pd loading in (a). c) The conversion versus time plots at different areas of the PdNCF sheet at a 5.3 wt% loading. d) The average reaction rate versus area of PdNCF in (c). The average reaction rates in (b) and (d) were estimated from the conversion change between 30 and 60 min.

to that of the fresh PdNCF membrane, as observed in the cross-sectional SEM and TEM images (Figure S10, Supporting Information). Furthermore, the cross-sectional TEM images of the recovered PdNCF membrane reveal a uniform distribution of Pd NPs within the nanopores, with no signs of aggregation (Figure S10c,d, Supporting Information). The concentration of residual Pd collected from the entire reaction solution, as determined by ICP-OES analysis, was found to be none. The minute amount of Pd sometimes detected in less than 0.1 ppm can be attributed to catalyst detachment from the top/bottom surface or edges of the membrane rather than from its inner nanopores.

The amount of Pd used for each reaction batch can be quantified by the Pd loading and the area of the PdNCF membrane (**Figure 6**). The optimal conversion could be obtained by increasing the Pd loading in the membrane up to 7.5 wt%, which correlates with the trend in the average reaction rate (Figure 6a,b). The catalysts' quantities are proportional to the size of the PdNCF membrane sheet (Figure S5, Supporting Information). For example, a 50 μm-thick circular sheet of PdNCF-5.3 with a diameter of 2 cm contains ≈0.3 mg of Pd. Then, the reaction rates can be increased by simply increasing the area of the PdNCF membrane sheet (Figure 6c,d). Overall, our findings demonstrate that utilizing the NCF membrane as a host for metal nanocatalysts in chemical reactions enables precise control of catalyst quantity and facilitates their long-term stable and recyclable use.

We further explored the effectiveness of the PdNCF for dechlorination of 2-chlorophenol and 2,4-dichlorophenol (DCP) in a batch reaction mode (Table S1, Supporting Information). The C—Cl bond at the ortho-position was less reactive than that at the para-position. Phenol was eventually obtained as the final product from the hydrodechlorination of 2,4-DCP.[47]

The specific activity and turnover frequency (TOF) for the hydrodechlorination reaction with the PdNCF and other nanopore-supported Pd catalyst systems appeared within an order of range. (Table S2, Supporting Information).[48–51] Nevertheless, it is uncertain that the activities for the different nanostructure and membrane configurations can be compared directly. Since molecular transport and diffusion may become limiting factors to the catalytic reaction in the nanopore, using a forced flow system is desirable.


© 2024 The Authors. Small published by Wiley-VCH GmbH

16136829, 2024, 29, Downloaded from https://onlinelibrary.wiley.com/doi/10.1002/smll.202309490 by Gwangju Institute Of Science, Wiley Online Library on [01/04/2026]. See the Terms and Conditions (https://onlinelibrary.wiley.com/terms-and-conditions) on Wiley Online Library for rules of use; OA articles are governed by the applicable Creative Commons License

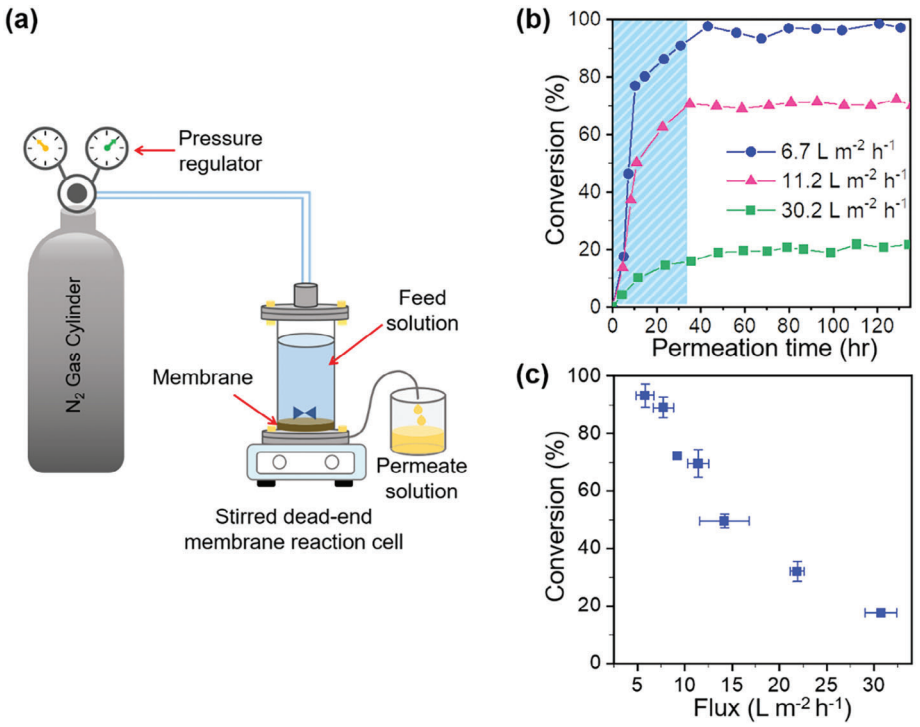


**Figure 7.** Continuous flow HDC reaction with the PdNCF membrane nanoreactor. a) Schematic illustration of the continuous pressurized flow HDC reaction with PdNCF membrane. b) Conversion monitored for 140 h of permeation (The initial stabilization period during 30 h is shaded in the graph). c) The conversion in the permeate at different fluxes of the reaction mixture. The feed solution contains 4-CP (0.5 mmol), HCOOK (30 mmol), and $Et_3N$ (1.0 mmol) in EtOH and $H_2O$ (1:1, 100 mL). PdNCF-5.3 (1.53 $cm^2$) was placed in the cell while maintaining the temperature at 40 °C with a temperature-controlled jacket.

### *2.2.2. Continuous-Flow Catalytic Reaction with PdNCF*

Taking advantage of the free-standing membrane materials and the immobilized active Pd NPs, we successfully conducted a continuous-flow HDC reaction using the PdNCF membrane (**Figure 7**). In the continuous-flow HDC setup depicted in Figure 7a, the reactant solution was pressurized to flow through the nanopores of the PdNCF membrane. The reaction must be progressed by one-time passage through a single 50 µm-thick membrane. This approach combines the benefits of continuous flow chemistry and heterogeneous catalysis, offering a versatile methodology that enables control over fluid velocity and enhances mass transfer.[52–57] Figure 7b demonstrates the remarkable stability and performance of the PdNCF membrane nanoreactor, maintaining ≈96% conversion even after 100 h of continuous operation at a solution flux of ≈7.0 L $m^{-2}$ $h^{-1}$, without any noticeable decline in activity. The extended stability is crucial for the PdNCF for continuous flow reactions. The essential advantage of continuous flow reactions is the ability to control the flux of feed solutions, which regulates the conversion in the permeate solution. For the HDC reaction, the conversion reached the maximum at the flux smaller than 7.0 L $m^{-2}$ $h^{-1}$, as shown in Figure 7c.

## 3. Conclusion

Our study emphasizes the potential of metal nanocatalyst-loaded membranes with 3D nanopores as a versatile and effective platform for catalytic nanoreactors. By incorporating ultrafine Pd nanoparticles into the polyurea network-based 3D-continuous NCF membranes, we harness the inherent advantages provided by their 3D nanoporous channels. These channels not only serve as efficient adsorption sites for metal nanocatalysts but also create controlled environments conducive to catalytic reactions. An essential advantage of our 3D nanoporous membrane-based approach is its precise control over the amount, size, and distribution of metal nanocatalysts. By adjusting catalyst loading and membrane area, we can easily regulate the quantity of catalyst used in a reaction. To showcase the performance of our system, we successfully apply the PdNCF membrane in a hydrodechlorination reaction. The catalysts housed within the nanopores exhibit exceptional long-term stability without aggregation, making them suitable for both batch and continuous flow reactions. Furthermore, we demonstrate the ability to optimize catalytic performance in continuous flow reactions by manipulating the flux of the reactant solution across the membrane. The metal nanocatalyst-loaded 3D nanoporous membrane nanoreactor offers a sustainable solution for supported metal catalysts, boasting stability, reusability, and the ability to achieve quantitative preparation without excessive metal usage. Additionally, the system enables precise control over the amount and distribution of catalyst within the nanoporous structure, as well as control over process conditions in both batch and flow modes. These attributes hold significant potential for maximizing the productivity and selectivity of catalytic reactions.


© 2024 The Authors. Small published by Wiley-VCH GmbH

16136829, 2024, 29, Downloaded from https://onlinelibrary.wiley.com/doi/10.1002/smll.202309490 by Gwangju Institute Of Science, Wiley Online Library on [01/04/2026]. See the Terms and Conditions (https://onlinelibrary.wiley.com/terms-and-conditions) on Wiley Online Library for rules of use; OA articles are governed by the applicable Creative Commons License

## 4. Experimental Section

*Materials*: Tetrakis(4-aminophenyl)methane (TAPM) was synthesized following a previously reported method.[58] Hexamethylene diisocyanate (HDI, 99% purity, Sigma–Aldrich) was freshly distilled under reduced pressure. An anhydrous grade of N,N-dimethylformamide (DMF, Sigma–Aldrich) was used as a solvent for the polymerization to obtain the UN sol. Polyethylene glycol (PEG, Sigma–Aldrich) with a number-average molecular weight ($M_n$) of 35000 was employed as a porogenic agent in obtaining the NCF membrane. Palladium acetate ($Pd(OAc)_2$, ≥99.9% purity, trace metals basis) and sodium borohydride ($NaBH_4$, 99% purity) were purchased from Sigma–Aldrich and used without further purification. Other materials were obtained from Sigma-Aldrich and were used as received.

*Synthesis of Urea Network (UN) Sols and NCF Membranes*: The sol of the urea-based network (UN) was synthesized by polymerizing TAPM and HDI in DMF at a concentration of 0.04 g $mL^{-1}$, following a previously reported method.[25] For the preparation of the NCF membrane, PEG was mixed with the UN sol, and subsequent extraction of PEG was carried out according to the previously reported procedure.[27,28] Specifically, PEG was added to the UN sol at a weight ratio of 60/40 (PEG/UN) and stirred for 1 h at 60 °C. The resulting PEG/UN mixed sol was then cast onto glass plates, and the solvent was evaporated through stepwise heating: 1 h at 50 °C, followed by 8 h at 80 °C. The NCF membrane was obtained by extracting the blend membrane with water to remove the soluble PEG component.

*Preparation of PdNCF*: A dried NCF membrane was immersed in a solution of $Pd(OAc)_2$ in acetone with concentrations ranging from 0.1 to 30 mM. The mixture was stirred at room temperature for 6 h. After removing the membrane from the precursor solution, it was washed with acetone to remove the residual $Pd(OAc)_2$ on the membrane's outer surface. Subsequently, the sample was dried under a nitrogen atmosphere at 70 °C for 6 h. Next, the dried membrane was immersed in a freshly prepared ice-cold aqueous $NaBH_4$ solution with a concentration of 20 mM for 30 min. The resulting PdNCF membranes were washed with water and dried under vacuum at 60 °C for 12 h. The PdNCF catalysts were designated as PdNCF-X, where X represents the Pd loading in weight percent (wt%).

*Adsorption of $Pd(OAc)_2$ onto the NCF Membrane*: The quantification of the adsorbed $Pd(OAc)_2$ per unit weight of the NCF film ($q_e$, mmol $g^{-1}$) was carried out using UV–vis spectroscopy based on the absorbance of the $Pd(OAc)_2$ solution at a wavelength of 462 nm. Dry NCF membranes with a defined mass of ≈0.1 g were immersed in $Pd(OAc)_2$ solutions of various concentrations, ranging from 0.5 to 20 mmol $L^{-1}$, for 6 h. The $q_e$ value was calculated using the following equation:

$$q_e = \frac{(C_0 V_0 - C_e V_e)}{m} \quad (1)$$

where $C_0$ and $C_e$ (mmol $L^{-1}$) are the initial and equilibrium concentrations of the $Pd(OAc)_2$ solution, respectively. $V_0$ and $V_e$ (L) are the volume of the $Pd(OAc)_2$ solution at initial and equilibrium state, respectively. $m$ (g) is the dry weight of the NCF membrane.

To predict the adsorption kinetics, the Langmuir adsorption isotherm was fitted using the following equation.[59]:

$$q_e = \frac{q_{max} K_L C_e}{1 + K_L C_e} \quad (2)$$

The linear form of the Langmuir equation is expressed as:

$$\frac{C_e}{q_e} = \frac{1}{K_L C_e} + \frac{1}{q_{max}} C_e \quad (3)$$

where $q_{max}$ (mmol $g^{-1}$) is the maximum adsorption capacity of the system. $K_L$ (L $mmol^{-1}$) is the Langmuir constant.

*Hydrodechlorination Batch Reaction*: In a typical batch reaction, a 100 mL two-neck round-bottom flask was prepared with a magnetic bar and fitted with a rubber septum. A mixture of HCOOK (6 mmol) and $Et_3N$ (0.8 mmol) dissolved in water (10 mL) was added to the flask. Then, a PdNCF-5.3 sheet (containing 1 mg of Pd over a 10.7 $cm^2$ area) was introduced to the flask and stirred at 40 °C for 30 min under a nitrogen atmosphere. Subsequently, 4-CP (0.4 mmol) in EtOH (10 mL) was added to the mixture. At specified time intervals, aliquots of the reaction solution were syringed out and extracted with diethyl ether (4 × 5 mL), and the combined extracts were washed with a brine solution. The conversion was estimated using gas chromatography coupled with a mass spectroscopic detector (GC-MS), employing an Rtx-1 column (30 m × 0.25 mm ID × 0.25 µm). Dodecane was utilized as the internal standard for quantitative analysis. After the reaction, the PdNCF membrane was separated from the solution and rinsed with water and EtOH. The recovered membrane was then immersed in a fresh reactant solution. Multiple reactions for seven cycles were conducted and monitored using the same procedure. For the SEM and TEM measurements of the recovered membranes after reactions, the membranes were washed with water and EtOH and then dried at 60 °C in a vacuum for 12 h.

*Hydrodechlorination Flow Reaction*: In a typical flow HDC reaction of 4-CP, a feed solution consisting of 4-CP (0.5 mmol), HCOOK (30 mmol), and $Et_3N$ (1.0 mmol) dissolved in a mixture of EtOH and $H_2O$ (1:1, 100 mL) was used. The PdNCF-5.3 catalyst, containing 0.3 mg of Pd over a 1.53 $cm^2$ area, was placed in a high-pressure cell (Sterlitech HP4750 stirred cell; Kent, USA) equipped with a homemade membrane holder designed for smaller membrane sizes (diameter = 13 mm). The active membrane area for permeation was $6.4 \times 10^{-5}$ $m^2$. The cell was equipped with a temperature-controlled jacket. The reaction cell was connected to a nitrogen gas (99.999%) source with a pressure regulator, which drove the feed solution through the membrane sheet. At 40 °C, the reaction stabilization time establishing steady-state conditions was ≈30 h. The permeated solution was taken periodically to analyze the conversion using GC-MS. The flux (ranging from 7.0 to 33 L $m^{-2}$ $h^{-1}$) was adjusted by varying gas pressures (1.0–5.0 bar) to investigate its effect on the reaction conversion.

*Characterization*: The transmission electron microscopy (TEM) was performed using a JEOL LTD model JEM-2100F. Ultrathin TEM specimens with a thickness of 80–100 nm were prepared using the PT-X/PT-XL PowerTome Ultramicrotomes from RMC Boeckeler. The TEM images were obtained without staining the samples. Scanning electron microscopy (SEM) images were obtained using a JEOL JSM-6700 system. Before SEM measurement, the membranes were dried at 100 °C under vacuum. The samples for cross-section analysis were prepared by breaking the membrane after dipping in liquid nitrogen for 5 min. The pieces were coated with platinum using a sputtering process before SEM imaging. $N_2$ adsorption–desorption isotherms were determined at 77 K using a Micromeritics ASAP 2020 Analyzer. Before the analysis, the samples were degassed at 100 °C for 12 h. The specific Brunauer–Emmett–Teller (BET) surface area, pore volume, and Barrett–Joyner–Halenda (BJH) pore size distribution were determined using ASAP 2020 ver 3.00 software. UV–vis spectra of the $Pd(OAc)_2$ solutions were acquired in the 200–650 nm range using a Mega-800 UV–vis spectrometer from Scinco. The Pd loading in each PdNCF membrane catalyst was obtained using an inductively coupled plasma optical emission spectrometer (ICP-OES) with the OPTIMA 8300 model. The quantitative analysis was performed with the characteristic Pd peak at 340.458 nm. X-ray photoelectron spectroscopy (XPS) analysis of the PdNCF membrane was conducted using a Thermo VG Scientific, VG Multilab 2000 instrument. The analysis utilized Al $K_\alpha$ X-ray radiation as the excitation source. X-ray Diffraction (XRD) analysis was performed using an X'Pert PRO Multi-Purpose X-Ray Diffractometer from PANalytical Co., England. The instrument employed a Cu 2 kW X-ray source (maximum 60 kV 55 $mA^{-1}$) for the analysis.

## Supporting Information

Supporting Information is available from the Wiley Online Library or from the author.


© 2024 The Authors. Small published by Wiley-VCH GmbH

16136829, 2024, 29, Downloaded from https://onlinelibrary.wiley.com/doi/10.1002/smll.202309490 by Gwangju Institute Of Science, Wiley Online Library on [01/04/2026]. See the Terms and Conditions (https://onlinelibrary.wiley.com/terms-and-conditions) on Wiley Online Library for rules of use; OA articles are governed by the applicable Creative Commons License

## Acknowledgements

J.-W.P. conceived the idea and ran the project. D.J. performed the main experiments, including synthesizing the Pd NCF membrane system and analyzing the reaction data. W.O. performed the synthesis and characterization of NCF membranes. All authors contributed to the writing of the manuscript and approved the final version of the manuscript. This research was supported by a National Research Foundation of Korea (NRF) grant funded by the Korean government (NRF-2021R1A2C2011530).

## Conflict of Interest

The authors declare no conflict of interest.

## Data Availability Statement

The data that support the findings of this study are available from the corresponding author upon reasonable request.

## Keywords

hydrodechlorination, nanoporous membrane, nanoreactor, palladium nanocatalyst

Received: October 19, 2023
Revised: April 7, 2024
Published online: April 23, 2024

[1] S. H. Petrosko, R. Johnson, H. White, C. A. Mirkin, *J. Am. Chem. Soc.* **2016**, *138*, 7443.
[2] M. Sanles-Sobrido, M. Perez-Lorenzo, B. Rodriguez-Gonzalez, V. Salgueirino, M. A. Correa-Duarte, *Angew. Chem., Int. Ed.* **2012**, *51*, 3877.
[3] X. Q. Kong, K. Zong, S. S. Lee, *Chem. Mater.* **2019**, *31*, 4953.
[4] W. Jia, C. Hu, Y. Wang, Y. Gu, G. Qian, X. Du, L. Wang, Y. Liu, J. Cao, S. Zhang, S. Yan, P. Zhang, J. Ma, H.-Y. Chen, S. Huang, *Nat. Commun.* **2021**, *12*, 5811.
[5] A. N. Khlobystov, *ACS Nano* **2011**, *5*, 9306.
[6] R. J. White, R. Luque, V. L. Budarin, J. H. Clark, D. J. Macquarrie, *Chem. Soc. Rev.* **2009**, *38*, 481.
[7] L. Q. Song, W. Y. Shi, C. Lu, *Anal. Chem.* **2016**, *88*, 8188.
[8] A. Phan, A. Striolo, *J. Phys. Chem. Lett.* **2020**, *11*, 1814.
[9] K. J. Lee, S. H. Min, J. Jang, *Small* **2010**, *6*, 2378.
[10] J. Liu, S. Z. Qiao, J. S. Chen, X. W. Lou, X. R. Xing, G. Q. Lu, *Chem. Commun.* **2011**, *47*, 12578.
[11] Y. Yang, X. Liu, X. B. Li, J. Zhao, S. Y. Bai, J. Liu, Q. H. Yang, *Angew. Chem., Int. Ed.* **2012**, *51*, 9164.
[12] S. Tevet, S. S. Wagle, G. Slor, R. J. Amir, *Macromolecules* **2021**, *54*, 11419.
[13] S. Y. Liu, J. V. M. Weaver, M. Save, S. P. Armes, *Langmuir* **2002**, *18*, 8350.
[14] L. M. Bronstein, Z. B. Shifrina, *Chem. Rev.* **2011**, *111*, 5301.
[15] R. M. Crooks, M. Q. Zhao, L. Sun, V. Chechik, L. K. Yeung, *Acc. Chem. Res.* **2001**, *34*, 181.
[16] Q.-L. Zhu, Q. Xu, *Chem* **2016**, *1*, 220.
[17] P. Munnik, P. E. de Jongh, K. P. de Jong, *Chem. Rev.* **2015**, *115*, 6687.
[18] E. A. Jackson, M. A. Hillmyer, *ACS Nano* **2010**, *4*, 3548.
[19] G. Hyun, J. T. Song, C. Ahn, Y. Ham, D. Cho, J. Oh, S. Jeon, *Proc. Natl. Acad. Sci. USA* **2020**, *117*, 5680.
[20] M. H. Tang, J. Deng, M. M. Li, X. F. Li, H. R. Li, Z. R. Chen, Y. Wang, *Green Chem.* **2016**, *18*, 6082.
[21] P. K. Su, C. H. Chang, Y. M. Sun, C. C. Hu, J. Y. Lai, Y. L. Liu, *J. Membr. Sci.* **2019**, *586*, 267.
[22] B. A. Pulido, C. Waldron, M. G. Zolotukhin, S. P. Nunes, *J. Membr. Sci.* **2017**, *539*, 187.
[23] I. Pinnau, B. D. Freeman, *ACS. Symp. Ser.* **2000**, *744*, 1.
[24] B. P. Tripathi, N. C. Dubey, S. Choudhury, P. Formanek, M. Stamm, *Adv. Mater. Interfaces* **2015**, *2*, 1500097.
[25] S. Y. Moon, J. S. Bae, E. Jeon, J. W. Park, *Angew. Chem., Int. Ed.* **2010**, *49*, 9504.
[26] W. Oh, J. W. Park, *ACS Appl. Mater. Interfaces* **2019**, *11*, 32398.
[27] J. S. Bae, E. Jeon, S. Y. Moon, W. Oh, S. Y. Han, J. H. Lee, S. Y. Yang, D. M. Kim, J. W. Park, *Angew. Chem., Int. Ed.* **2016**, *55*, 11495.
[28] W. Oh, D. Jeong, J. W. Park, *Adv. Mater. Interfaces* **2023**, *10*, 2300185.
[29] K. Karami, Z. K. Moghadam, M. Hosseini-Kharat, *Catal. Commun.* **2014**, *43*, 25.
[30] A. Dumas, A. Peramo, D. Desmaële, P. Couvreur, *Chimia* **2016**, *70*, 252.
[31] L. C. C. Vieira, M. W. Paixão, G. A. Corrêa, *Tetrahedron Lett.* **2012**, *53*, 2715.
[32] B. Aguila, Q. Sun, H. C. Cassady, C. Shan, Z. Liang, A. M. Al-Enizic, A. Nafadyc, J. T. Wright, R. W. Meulenberg, S. Ma, *Angew. Chem., Int. Ed.* **2020**, *59*, 19618.
[33] M. L. Rahman, H. B. Mandal, S. M. Sarkar, M. N. Kabir, E. M. Farid, S. E. Arshad, B. Musta, *J. Macromol. Sci., Part A: Pure Appl. Chem.* **2016**, *53*, 515.
[34] H. Seto, T. Yoneda, T. Morii, Y. Hoshino, Y. Miura, T. Murakami, *AIChE J.* **2015**, *61*, 582.
[35] X. L. Pei, Y. Deng, Y. Li, Y. G. Huang, K. Yuan, J. F. Lee, T. S. Chan, J. P. Zhou, A. W. Lei, L. N. Zhang, *Nanoscale* **2018**, *10*, 14719.
[36] H. C. Li, W. J. Liu, H. X. Han, H. Q. Yu, *J. Mater. Chem. A* **2016**, *4*, 11680.
[37] L. J. Wang, J. Zhang, X. Zhao, L. L. Xu, Z. Y. Lyu, M. Lai, W. Chen, *RSC Adv.* **2015**, *5*, 73451.
[38] L. Q. Xu, W. Q. Zhang, Y. W. Ding, W. C. Yu, J. Y. Xing, F. Q. Li, Y. T. Qian, *J. Cryst. Growth* **2004**, *273*, 213.
[39] B. P. Chaplin, M. Reinhard, W. F. Schneider, C. Schuth, J. R. Shapley, T. J. Strathmann, C. J. Werth, *Environ. Sci. Technol.* **2012**, *46*, 3655.
[40] R. R. Li, Z. H. Zhou, J. J. Chen, S. T. Wang, J. L. Zheng, C. Chu, J. Zhao, H. J. Fan, D. M. Han, *New J. Chem.* **2019**, *43*, 6659.
[41] M. J. Detisch, T. J. Balk, D. Bhattacharyya, *Ind. Eng. Chem. Res.* **2018**, *57*, 4420.
[42] M. K. Anwer, R. A. Porter, A. F. Spatola, *Int. J. Peptide Protein Res.* **1987**, *30*, 489.
[43] S. Rajagopal, A. F. Spatola, *Appl. Catal. A* **1997**, *152*, 69.
[44] A. Pavlova, E. Rosler, E. J. Meijer, *ACS Catal.* **2016**, *6*, 5350.
[45] Y. H. Luo, Y. H. Cai, X. X. Long, D. D. Zhou, C. Zhou, B. E. Rittmann, *Environ. Sci Technol.* **2022**, *56*, 4447.
[46] P. Wang, X. L. Shi, C. H. Fu, X. J. Li, J. X. Li, X. S. Lv, Y. H. Chu, F. Dong, G. M. Jiang, *Nanoscale* **2020**, *12*, 843.
[47] Z. Sun, H. Shen, X. Wei, X. Hu, *Chem. Eng. J.* **2014**, *241*, 433.
[48] B. J. Yao, J. T. Li, N. Huang, J. L. Kan, L. Qiao, L. G. Ding, F. Li, Y. B. Dong, *ACS Appl. Mater. Interfaces* **2018**, *10*, 20448.
[49] Y. S. Liu, Z. P. Dong, X. L. Li, X. D. Le, W. Zhang, J. T. Ma, *RSC Adv.* **2015**, *5*, 20716.
[50] C. Ruiz-García, F. Heras, L. Calvo, N. Alonso-Morales, J. J. Rodríguez, M. A. Gilarranz, *Ind. Eng. Chem. Res.* **2019**, *58*, 4355.
[51] J. Nieto-Sandoval, E. Gomez-Herrero, M. Munoz, Z. M. de Pedro, J. A. Casas, *Appl. Catal. B-Environ.* **2021**, *293*, 120235.
[52] V. Hessel, D. Kralisch, N. Kockmann, T. Noel, Q. Wang, *ChemSusChem* **2013**, *6*, 746.
[53] J. Yoshida, Y. Takahashi, A. Nagaki, *Chem. Commun.* **2013**, *49*, 9896.


© 2024 The Authors. Small published by Wiley-VCH GmbH

16136829, 2024, 29, Downloaded from https://onlinelibrary.wiley.com/doi/10.1002/smll.202309490 by Gwangju Institute Of Science, Wiley Online Library on [01/04/2026]. See the Terms and Conditions (https://onlinelibrary.wiley.com/terms-and-conditions) on Wiley Online Library for rules of use; OA articles are governed by the applicable Creative Commons License

[54] K. Jahnisch, V. Hessel, H. Lowe, M. Baerns, *Angew. Chem., Int. Ed.* **2004**, *43*, 406.
[55] J. Zakrzewski, P. Yaseneva, C. J. Taylor, M. J. Gaunt, A. A. Lapkin, *Org. Process Res. Dev.* **2023**, *27*, 649.
[56] I. Sadeghi, E. Y. Liu, H. M. Yi, A. Asatekin, *ACS Appl. Nano. Mater.* **2019**, *2*, 5233.
[57] Y. Chen, S. Q. Fan, J. J. Chen, L. Deng, Z. Y. Xiao, *ACS Appl. Mater. Interfaces* **2022**, *14*, 9106.
[58] P. Ganesan, X. N. Yang, J. Loos, T. J. Savenije, R. D. Abellon, H. Zuilhof, E. J. R. Sudholter, *J. Am. Chem. Soc.* **2005**, *127*, 14530.
[59] I. Langmuir, *J. Am. Chem. Soc.* **1918**, *40*, 1361.

 © 2024 The Authors. Small published by Wiley-VCH GmbH

16136829, 2024, 29, Downloaded from https://onlinelibrary.wiley.com/doi/10.1002/smll.202309490 by Gwangju Institute Of Science, Wiley Online Library on [01/04/2026]. See the Terms and Conditions (https://onlinelibrary.wiley.com/terms-and-conditions) on Wiley Online Library for rules of use; OA articles are governed by the applicable Creative Commons License